

In-plane field-induced vortex liquid correlations in underdoped $\text{Bi}_2\text{Sr}_2\text{CaCu}_2\text{O}_{8+\delta}$

Panayotis Spathis, Marcin Konczykowski, and Cornelis J. van der Beek

Laboratoire des Solides Irradiés, CNRS UMR 7642 & CEA/DSM/DRECAM, Ecole Polytechnique, 91128 Palaiseau, France

Piotr Gierłowski

Institute of Physics of the Polish Academy of Sciences, 32/46 Aleja Lotników, 02-668 Warsaw, Poland

Ming Li, Peter H. Kes

Kamerlingh Onnes Laboratorium, Rijksuniversiteit Leiden, P.O. Box 9506, 2300 RA Leiden, The Netherlands

(Dated: October 7, 2018)

The effect of a magnetic field component parallel to the superconducting layers on longitudinal Josephson plasma oscillations in the layered high temperature superconductor $\text{Bi}_2\text{Sr}_2\text{CaCu}_2\text{O}_{8+\delta}$ is shown to depend on the thermodynamic state of the underlying vortex lattice. Whereas the parallel magnetic field component depresses the Josephson Plasma Resonance (JPR) frequency in the vortex solid phase, it may enhance it in the vortex liquid. There is a close correlation between the behavior of microwave absorption near the JPR frequency and the effectiveness of pancake vortex pinning, with the enhancement of the plasma resonance frequency occurring in the absence of pinning, at high temperature close to the vortex melting line. An interpretation is proposed in terms of the attraction between pancake vortices and Josephson vortices, apparently also present in the vortex liquid state.

PACS numbers: 74.20.De, 74.25.Bt, 74.25.Dw, 74.25.Op, 74.25.Qt, 74.72.Hs

I. INTRODUCTION

The application of magnetic fields oblique to the superconducting planes of layered superconductors leads to novel vortex structures. Recent low-field scanning Hall probe¹ and Lorentz microscopy experiments² on single crystalline $\text{Bi}_2\text{Sr}_2\text{CaCu}_2\text{O}_{8+\delta}$ have demonstrated the attraction between Josephson vortex (JV) and pancake vortex (PV) stacks, induced by, respectively, the field components H^{\parallel} and H^{\perp} parallel and perpendicular to the layers. This attraction leads to the formation of the so-called combined lattice,³ observed earlier in Bitter decoration.⁴ In a $(H^{\parallel}, H^{\perp})$ phase diagram, the combined vortex lattice is delimited, as H^{\perp} is increased, by a first order vortex melting transition to a vortex liquid at $H_m^{\perp}(H^{\parallel})$.^{3,5,6,7,8} As H^{\parallel} is increased, there is another first order transition to a tilted PV lattice.⁸ However, the actual structure of the different phases near the melting and combined-to-tilted transition lines remains speculative.

Whereas surface-sensitive techniques^{1,2,3,4,5,6,7,8} can establish phase boundaries, deeper insight in the structure of the vortex ensemble may be obtained from a bulk probe such as Josephson Plasma Resonance (JPR).⁹ In analogy to JPR in a single junction, a microwave electric field applied perpendicularly to the superconducting layers of the $\text{Bi}_2\text{Sr}_2\text{CaCu}_2\text{O}_{8+\delta}$ compound (*i.e.* parallel to the crystalline *c*-axis) induces a collective oscillation of Cooper pairs at the frequency $f_{pl} = (sj_c^c/2\pi\Phi_0\varepsilon)^{1/2}$. Here, j_c^c is the maximum *c*-axis (Josephson) critical current density, $\Phi_0 = h/2e$ is the flux quantum, $s = 1.5$ nm the interlayer spacing, and ε the dielectric constant. At the JPR frequency, the kinetic energy hf_{pl} of the tunneling pairs is equal to the potential energy engendered by the time-periodic difference of the gauge-invariant superconducting order parameter phase ϕ between layers.^{10,11}

In the absence of a magnetic field component parallel to the superconducting layers, the JPR frequency squared is proportional to the time- and disorder-averaged cosine of the difference of ϕ in adjacent layers $n, n+1$:^{11,12}

$$f_{pl}^2(\mathbf{B}, T) = f_{pl}^2(0, T) \langle \cos \phi_{n,n+1} \rangle \equiv f_{pl}^2(0, T) \mathcal{C}. \quad (1)$$

Since the spatial configuration of $\phi(\mathbf{r})$ is determined by the vortex distribution inside the sample, JPR is sensitive to the local structure of different vortex states.¹¹

In the presence of a parallel magnetic field component, the *c*-axis electric field E^{\perp} used to excite the JPR leads to periodic oscillations of the Josephson vortex lattice. Very recently, Koshelev explored a solution of coupled equations for plasma oscillations and JV lattice motion.¹³ In the limit of a dense JV lattice, $B^{\parallel} > B_d = \Phi_0/2\pi\gamma s^2$, the frequency of longitudinal plasma oscillations with $q_{\perp} = 0$ (homogeneous displacement $u(\mathbf{r})$ of the JV lattice along the layers) is

$$f_{pl} = f_{pl}(H=0) \sqrt{2 \langle \cos \phi_{0n} \rangle + \frac{B^{\parallel}}{2B_d}} \quad (B^{\parallel} > B_d). \quad (2)$$

The JPR frequency increases with increasing parallel field, as the coupled system stiffens due to the increasing JV density. In the above, $B^{\parallel} = \mu_0 H^{\parallel}$, $\mu_0 = 4\pi \times 10^{-7} \text{ Hm}^{-1}$, $\gamma \equiv \lambda_c/\lambda_{ab}$ is the anisotropy of the *c*-axis and in-plane penetration depths, and

$$\langle \cos \phi_{0n} \rangle = \frac{1}{2} \left[4 + \left(\frac{s}{\lambda_{ab}} \right)^2 \right] \frac{B_d}{B^{\parallel}} \quad (B^{\parallel} \gtrsim 2B_d) \quad (3)$$

is the average cosine of the phase

$$\phi_{0n} = 2\pi y/c_y + \pi n + \alpha_n(y) \quad (B^{\parallel} > B_d) \quad (4)$$

in layer n . The phase consists of a monotonously increasing contribution along the in-plane coordinate y ,

arising from the nearly homogeneous H^{\parallel} component, an in-plane oscillating contribution $\alpha_n(y)$, and an out-of-plane stepwise contribution. The latter two terms reflect the structure of the JV lattice. The in-plane JV spacing is $c_y = \Phi_0/2\pi s B^{\parallel}$ in the dense limit, while $c_y = \sqrt{\beta\gamma\Phi_0/B^{\parallel}}$ in the opposite, dilute limit ($\beta \equiv 2/\sqrt{3}$). Apart from the $q_{\perp} = 0$ mode, a further, low-frequency mode with $q_{\perp} = \pi/s$ and $f_{min} \approx 2f_{pl}(H=0)\sqrt{B_d/B^{\parallel}}$ is also predicted.¹³ This corresponds to antiphase motion of JV's in adjacent layers.

Experimentally, Josephson Plasma Resonance with a magnetic field applied obliquely to the superconducting planes of single crystalline $\text{Bi}_2\text{Sr}_2\text{CaCu}_2\text{O}_{8+\delta}$ has been studied by various authors.^{9,14,15,16,17} With the exception of Ref. 17, these studies were limited to low temperatures $T < 0.6T_c$ and $H^{\parallel} \gg H^{\perp}$, in the regime where the vortex liquid is the melt of the *tilted* PV lattice. The following results have been obtained. In the vortex liquid, the perpendicular field component $H_{JPR}^{\perp} = H^{\perp}(f = f_{pl})$ at which the main JPR absorption peak occurs was found to decrease with increasing H^{\parallel} .^{14,15,16} This is understood by the theory for a “homogeneous” vortex liquid without any interlayer PV correlations, developed in Ref. 11. Briefly, the short range of the interlayer phase correlations inhibits the formation of a JV lattice, and leads to a very high effective anisotropy γ . Only the homogeneously increasing part of the phase (4) remains; the JPR frequency decreases as the exponent of $H^{\parallel 2}$.^{15,18} As the field is oriented closely to the superconducting layers, a “re-entrance” of $H_{JPR}^{\perp}(H^{\parallel})$ occurs, such that H_{JPR}^{\perp} now increases with H^{\parallel} . This behavior was interpreted in terms of a model worked out by Bulaevskii *et al.* for the JV lattice in the dense limit, interacting with the PV lattice.^{16,19} The JPR frequency is thought to increase both as function of H^{\perp} and H^{\parallel} because of the larger JV lattice stiffness and the increasing JV-PV interaction (leading to a zig-zag PV lattice structure).¹⁹ A caveat of this model is that, at fields $(H^{\perp}, H^{\parallel})$ at which the increase of the JPR frequency is observed in $\text{Bi}_2\text{Sr}_2\text{CaCu}_2\text{O}_{8+\delta}$, there is no evidence for a JV lattice.⁸

In this paper, we explore microwave dissipation in the regime of high temperature and moderate field angles, $H^{\perp} \lesssim H^{\parallel} \lesssim \mu_0^{-1}B_d$, in which the vortex liquid arises from the first order melting of the *combined* lattice, that is, a vortex solid phase in which the presence of JV stacks has been established.^{3,6,7,8} In this regime, we find a clear correlation between the behavior of $f_{pl}(H^{\parallel})$ and the thermodynamic state of the PV lattice as well as with PV pinning by material defects. In particular, we show that while increasing H^{\parallel} in the vortex solid phase yields a modest decrease of f_{pl} , the JPR frequency in the vortex liquid phase close to the melting line is *enhanced* by the additional in-plane field. This is in agreement with data of Refs. 15, 17 and 20 that suggest an increase of both f_{pl} and the *c*-axis conductivity with increasing H^{\parallel} under similar experimental conditions. We conclude that in the regime under study the vortex liquid has a correlated character due to the persistence of Josephson vortices. Moreover, the sharp dependence of f_{pl} on PV density in the liquid reveals a boundary between this correlated

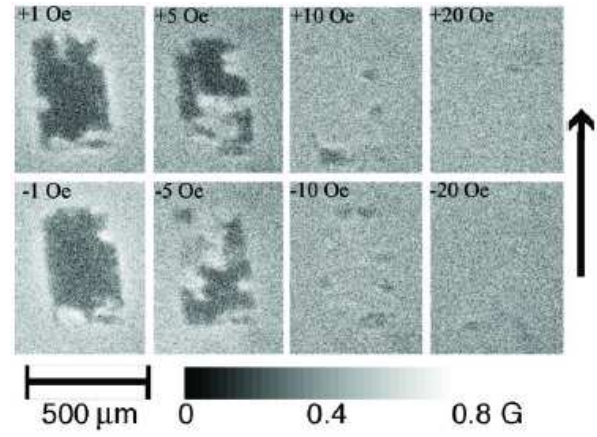


FIG. 1: Differential magneto-optical images of the underdoped $\text{Bi}_2\text{Sr}_2\text{CaCu}_2\text{O}_{8+\delta}$ single crystal ($0.28 \times 0.46 \times 0.04 \text{ mm}^3$) at $T = 60 \text{ K}$. An in-plane field $H^{\parallel} = 500 \text{ Oe}$ was applied in the direction of the arrow. Images were obtained by averaging 10 CCD frames taken at the field $H^{\perp} + \Delta H^{\perp}$ and subtracting the average of 10 frames taken at H^{\perp} . This procedure was repeated 100 times. The field modulation ΔH^{\perp} was 0.5 Oe. The intensity scale shows the magnitude of the ac component of the local induction, $\Delta B^{\perp} = B^{\perp}(H^{\perp} + \Delta H^{\perp}) - B^{\perp}(H^{\perp})$.

liquid and the homogeneous vortex liquid at higher fields.

II. EXPERIMENTAL DETAILS

Single crystals ($T_c = 72.4 \pm 0.6 \text{ K}$) were cut from a batch of underdoped $\text{Bi}_2\text{Sr}_2\text{CaCu}_2\text{O}_{8+\delta}$,²¹ and characterized using the differential magneto-optical technique (DMO).²² By taking the difference between the average of 10 consecutive magneto-optical images acquired at perpendicular fields $H^{\perp} + \Delta H^{\perp}$ and H^{\perp} , one obtains the local magnetic permeability at field modulation ΔH^{\perp} (Fig. 1). Underdoped $\text{Bi}_2\text{Sr}_2\text{CaCu}_2\text{O}_{8+\delta}$ being prone to significant disorder in oxygen distribution,²³ the DMO technique was used to select the most homogeneous crystals for further experiments. Nevertheless, some inhomogeneity in the penetration of perpendicular magnetic flux remains, as shown in Fig. 1. A clear dependence of the direction of flux penetration was observed, depending on the relative orientation of H^{\perp} and H^{\parallel} . The DMO technique was also used to detect the irreversibility line $B_{irr}(T)$, at which the permeability becomes unmeasurably small due to the demise of vortex pinning, both with $H^{\parallel} = 0$ and $H^{\parallel} = 500 \text{ Oe}$.

The local magnetization was measured using a microscopic Hall probe array.^{5,8} The first order melting field H_m^{\perp} of the vortex lattice was determined from the sharp paramagnetic peak that melting induces in the first and third harmonic of the transmittivity.^{6,8,24} The temperature dependence of the melting field in $H^{\parallel} = 0$ is well described by $H_m^{\perp} \sim A\Phi_0/\mu_0\gamma s\lambda_{ab}(\varepsilon_0 s/k_B T)$, where $\varepsilon_0 = \Phi_0^2/4\pi\mu_0\lambda_{ab}^2$, and $A \approx 1$.²⁵ The dependence of H_m^{\perp} on H^{\parallel} is in every way similar to that observed in optimally doped single crystalline $\text{Bi}_2\text{Sr}_2\text{CaCu}_2\text{O}_{8+\delta}$ (see Fig. 2). The melting field of the combined lattice fol-

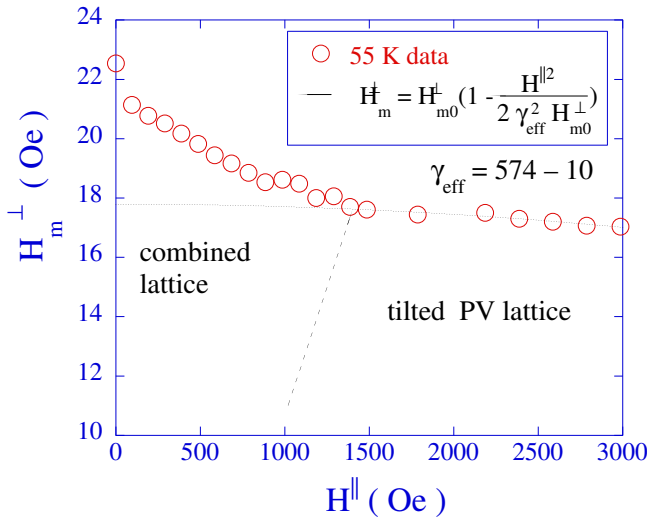


FIG. 2: First order vortex lattice melting field of the underdoped $\text{Bi}_2\text{Sr}_2\text{CaCu}_2\text{O}_{8+\delta}$ crystal of Fig. 1, at $T = 55$ K. As the in-plane field H^{\parallel} increases, H_m^{\perp} first decreases linearly. At high in-plane fields, the parabolic behavior $H_m^{\perp} \approx H_{m0}^{\perp} \left(1 - H^{\parallel 2} / 2\gamma_{\text{eff}}^2 H_{m0}^{\perp 2}\right)$ corresponding to the anisotropic London model is followed.⁸ The dashed line indicates the boundary between combined lattice and tilted pancake vortex lattice phases.

lows a linear H^{\parallel} -dependence, while the melting of the tilted PV lattice at high H^{\parallel} follows a parabolic dependence. From a fit of the latter to the anisotropic London model,⁸ we obtain an effective anisotropy parameter $\gamma^{\text{eff}} \approx 574 \pm 10$, close to the bare value $\gamma \approx 600$ obtained previously for underdoped $\text{Bi}_2\text{Sr}_2\text{CaCu}_2\text{O}_{8+\delta}$.¹²

The microwave dissipation was measured using the cavity perturbation technique.¹² Two different oxygen-free high-conductivity copper resonant cavities, with the TM_{010} mode at 19.2 GHz and 38.7 GHz respectively, were used in the measurements. The sample was glued in the center of the cavity end-plate so that the microwave electrical field E^{\perp} was perpendicular to the superconducting layers when the cavity was operated in the TM_{01i} resonant modes. For cavity I, the unloaded quality factors Q of five modes with $i = 0, \dots, 4$ were measured as a function of magnetic field and temperature, allowing us to probe the microwave dissipation in both the vortex liquid and vortex solid state during the same run. For cavity II, only the TM_{010} and TM_{011} modes were used. For all modes, the sample lateral dimensions (typically $< 500 \mu\text{m}$) were sufficiently small with respect to the cavity size for E^{\perp} to be considered homogeneous, and the microwave magnetic field to be negligible. This was checked by cutting the most important crystals in two, and remeasuring the microwave absorption (e.g., on the crystal of Fig. 1).

Two orthogonal coils were used to control H^{\parallel} and H^{\perp} independently. Measurements were carried out by first applying H^{\parallel} in the normal state, by setting the desired temperature, and then sweeping H^{\perp} . The misalignment of H^{\perp} did not exceed 1° , entailing a variation of H^{\parallel} of less than 2 Oe. The symmetry of the microwave re-

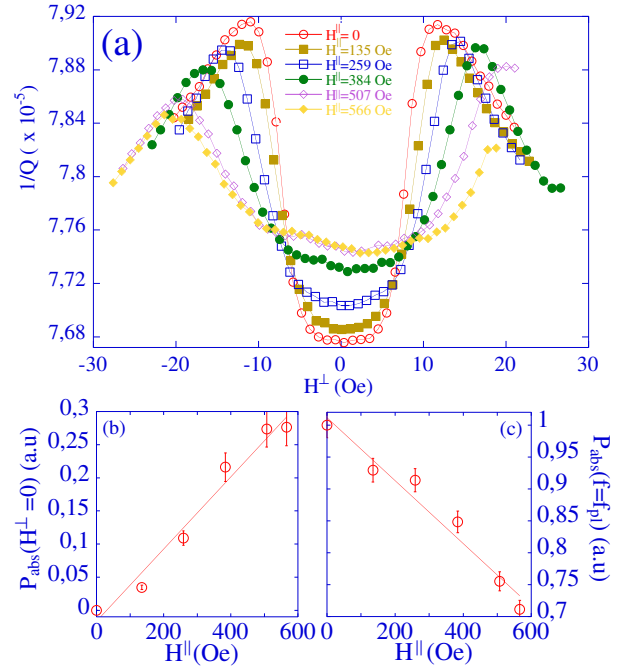


FIG. 3: (a) Magnetic-field dependence of the microwave absorption obtained during a sweep of the perpendicular field, for different in-plane fields at 66 K and 19.2 GHz. All data were taken during the same run, allowing for a quantitative comparison of the power absorption. The temperature was raised above T_c between runs with different in-plane fields. (b) Microwave losses for $H^{\perp} \approx 0$: $P_{\text{abs}}(H^{\perp} = 0) = [Q^{-1}(0, H^{\parallel}) - Q^{-1}(0, 0)] / [Q^{-1}(H_{JPR}^{\perp}, 0) - Q^{-1}(0, 0)]$. (c) Magnitude of the absorption at the JPR: $P_{\text{abs}} = [Q^{-1}(H_{JPR}^{\perp}, H^{\parallel}) - Q^{-1}(0, 0)] / [Q^{-1}(H_{JPR}^{\perp}, 0) - Q^{-1}(0, 0)]$.

sponse with respect to H^{\perp} and the absence of parasitic field components was checked by sweeping H^{\perp} up to the maximum positive value, from there down to the maximum negative value and back to zero.

III. RESULTS

Fig. 3(a) shows the microwave absorption at 66 K and 19.2 GHz during the H^{\perp} -sweeps, for different values of H^{\parallel} . For $H^{\perp} \approx 0$, the power absorption linearly increases with in-plane field [Fig. 3(b)]. Upon increasing H^{\perp} from zero, the absorption rises, and a clear maximum of Q^{-1} appears, corresponding to the excitation of the Josephson Plasma Resonance at $f = f_{pl}(H, T)$.^{9,10} The independence of the shape and position of the measured JPR peaks on sample size confirm that the longitudinal JPR mode is observed. Performing the measurement for non-zero parallel field component, one sees that the maximum of the absorption shifts to higher H^{\perp} as H^{\parallel} increases. The low- H^{\perp} flank of the absorption peak is progressively suppressed with H^{\parallel} , while the high-field tail is nearly H^{\parallel} -independent; concordantly, the absorption peak progressively diminishes in height [Fig. 3(c)].

The temperature evolution of the absorption during H^{\perp} -sweeps performed with an in-plane field $H^{\parallel} = 1$ kOe is depicted in Fig. 4. For temperatures above 61

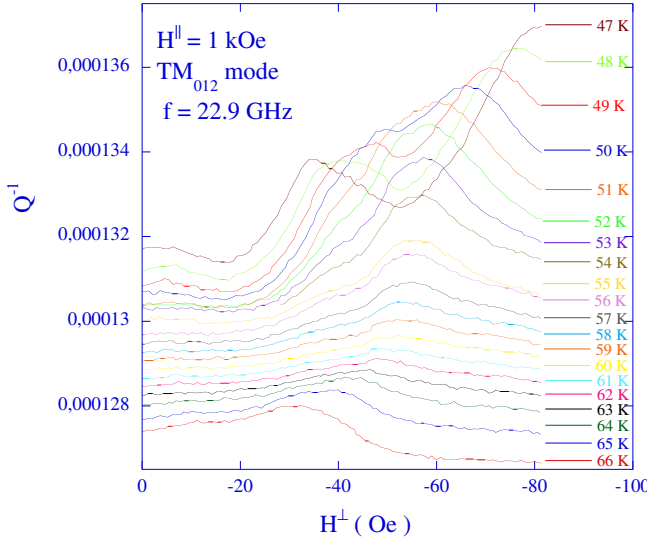


FIG. 4: (a) Dependence on perpendicular field H^\perp of the microwave absorption at 22.9 GHz, at different temperatures. The parallel field $H^\parallel = 1$ kOe. Data are plotted as one over the unloaded quality factor of the resonant cavity. At high temperatures, there is a single absorption maximum. At $T \lesssim 55$ K, a second, low H^\perp -peak appears. All field sweeps have been performed during a single run, with the sample being heated above T_c between different measurement temperatures. For clarity, successive curves have been displaced by $\Delta Q = 30$.

K, a single absorption maximum is observed, and the behavior at all investigated in-plane fields is that represented by Fig. 3(a). This peak corresponds to the “high temperature resonance” reported in Refs. 17,26. Its height decreases as function of H^\parallel and temperature. For $T \lesssim 61$ K and in-plane fields in excess of 600 Oe, a shoulder appears, that develops into a second, low-field absorption maximum as the temperature is lowered. The two low-temperature absorption peaks correspond to the reentrant “low temperature resonance” of Refs. 17,26. The magnitude of microwave absorption on the high-field branch of this “low-temperature resonance” is very weakly dependent on H^\parallel and nearly equal to that measured in $H^\parallel = 0$. Unlike previous reports,^{17,26} clear peaks in the absorption could not be observed when the magnetic field was perfectly aligned with the superconducting layers.

Fig. 5 collects the perpendicular field component $H_{JPR}^\perp \equiv H^\perp(f_{pl} = 22.9$ GHz) at which the JPR absorption maximum is located, for different magnitudes of the in-plane field. For this particular frequency, the main JPR peak occurs in the vortex liquid phase. Comparing the evolution of the JPR for different values of H^\parallel to the case where $H^\parallel \approx 0$, one can distinguish four different temperature regimes. Within 2 K of T_c , microwave absorption is very large and the resonant field cannot be identified (regime I). As the temperature is lowered, the JPR becomes observable. The JPR field sharply increases with decreasing T (regime II), and then slows down to a plateau (regime III). In this regime,

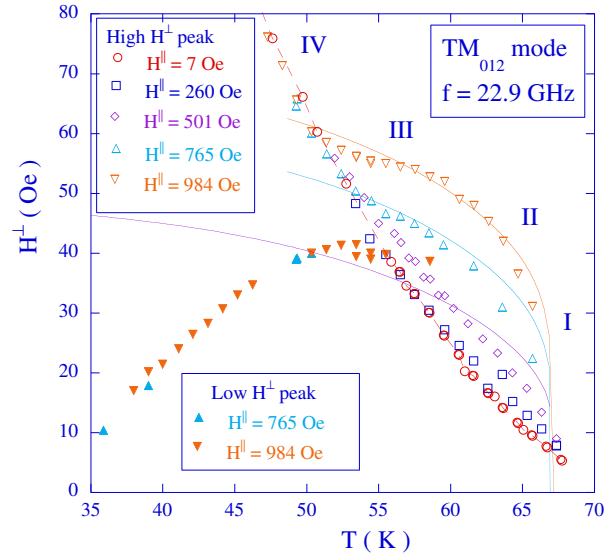


FIG. 5: Temperature dependence of JPR fields obtained for 22.9 GHz for various in-plane fields. Open symbols represent the dissipation peak measured at high perpendicular field, closed symbols represent the position of the low- H^\perp maximum observed for $H^\parallel > 500$ Oe. Drawn lines represent the boundary (5), evaluated with $\tilde{C} = 2.6$, at which phase correlations in the liquid have dropped back to their value in zero in-plane field. The dashed line is a guide to the eye representing the H_{JPR}^\perp -locus for $H^\parallel = 0$.

B_{JPR}^\perp increases nearly quadratically with H^\parallel (Fig. 6). We note that the upward shift of the lines of constant f_{pl} in regimes II and III implies the *increase of f_{pl} itself* when an in-plane field is applied and H^\perp is kept constant. Finally, at low T , H_{JPR}^\perp is smaller than it is for $H^\parallel = 0$ (regime IV). The observed decrease in this regime is larger for lower frequencies, *i.e.* higher temperatures, and is described by the high-temperature expansion.^{11,15,18}

In Fig. 7, we compare the position of B_{JPR}^\perp at three different frequencies to the main features of the vortex phase diagram. In the absence of an in-plane field [Fig. 7(a)], the JPR at 19.2 and 22.9 GHz occurs in the vortex liquid state. The application of a parallel field component leads to the increase of H_{JPR}^\perp and the four regimes described above. However, when the JPR occurs in the vortex solid, H_{JPR}^\perp shows a moderate decrease when an in-plane field is applied [Fig. 7(b)].

IV. DISCUSSION

The behavior of the field at which the JPR is excited can be summarized as follows. In the vortex solid phase, and in the vortex liquid at low temperature [regime IV, in Figs. 4 and 7(a)], H_{JPR}^\perp decreases as H^\parallel is increased. These regimes correspond to those parts of the (H, T) -phase diagram in which pinning of the pancake vortices due to material defects is strong. Notably, in underdoped $\text{Bi}_2\text{Sr}_2\text{CaCu}_2\text{O}_8$, which is characterized by the presence of numerous oxygen vacancies in the superconducting

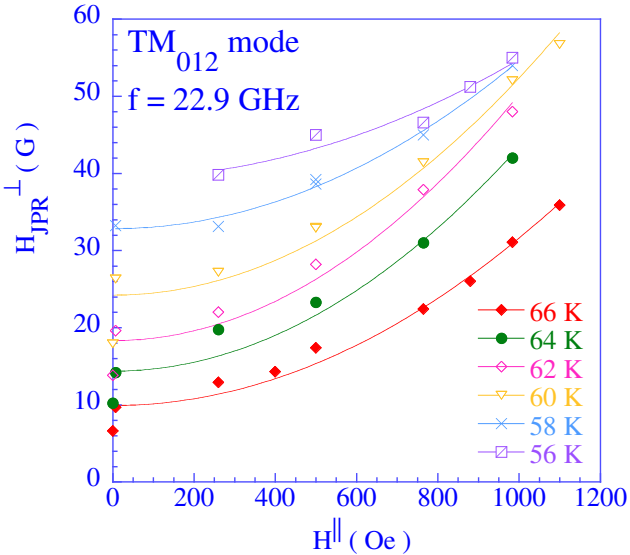


FIG. 6: In-plane field-dependence of H_{JPR}^{\perp} at 22.9 GHz.

CuO_2 -planes,²⁷ as well as substantial disorder in the oxygen distribution, one has strong pancake vortex pinning in the vortex solid phase.²³ On the other hand, the featureless DMO images above the first order melting line show that vortex pinning in the vortex liquid at high temperature is absent. Then, H_{JPR}^{\perp} dramatically increases with H^{\parallel} , signalling an increase of the Josephson plasma frequency.²⁸ In regime I, for $T > 67$ K, no features related to the JPR can be observed when a parallel field component is applied.

The above observations can be consistently explained by invoking the presence of Josephson vortices in both the vortex solid (combined lattice) *and* the vortex liquid phases, and their interaction with the microwave electrical field E^{\perp} and with pancake vortices. The interaction of JV's with E^{\perp} only is brought out by the absorption at $B^{\perp} = 0$. In our experimental configuration, the E^{\perp} induces a *c*-axis current that drives the JV's, thus producing flux-flow losses.^{15,26,29} The dissipated microwave power is proportional to $E^{\perp 2}/\rho_f \propto f^2 H_{\parallel}^2/\rho_f$, where ρ_f is the JV flux-flow resistivity. Experimentally, the dissipated power $\sim Q^{-1}$ is found to be linear in H^{\parallel} [Fig. 3(b)]. This implies the linearity of ρ_f with in-plane field, in full agreement with the prediction of Koshelev¹¹ and the experiments of Latyshev³⁰ in the dilute limit of the JV lattice, $B^{\parallel} < B_d$.

The effect of the PV lattice on JV motion was recently explored by Koshelev, Latyshev, and Konczykowski,³¹ who found that the attractive interaction between a moderate density of pancakes and the JV lattice induces significant damping of the JV motion and an increase of j_c^c in overdoped $\text{Bi}_2\text{Sr}_2\text{CaCu}_2\text{O}_8$ whiskers. Moreover, heavy-ion irradiation of the whiskers introduces defects that strongly pin the PV's, overwhelming the PV-JV attraction and re-establishing the JV mobility. We surmise that in our experiment, PV's in the vortex solid are strongly pinned; therefore, the microwave electric field drives large-amplitude JV oscillations. We then expect

the JPR frequency to be described by Eq. (2). The main effect of the PV lattice is a small random contribution to ϕ_{0n} arising from thermal fluctuations, and a concomitant reduction of $\langle \cos \phi_{0n} \rangle$ as a function of H^{\perp} . This entails the modest decrease of $H_{JPR}^{\perp}(H^{\parallel})$ that is experimentally observed.

We now turn to regimes II and III, in which H_{JPR}^{\perp} increases quadratically as function of H^{\parallel} . The increase of the characteristic frequency of this high temperature plasma mode was interpreted by Kakeya *et al.* as being due to the plasma wave propagation at $\mathbf{q} = (q_{\parallel} = 2\pi/c_y, q_{\perp} = \pi/s)$. The dispersion relation of the longitudinal plasma, $f_{pl} = f_{pl}(\mathbf{q} = 0)\sqrt{1 + \lambda_{ab}^2 q_{\perp}^2}$, would then be responsible for the observed H^{\parallel} dependence. However, the dispersion of the longitudinal plasma is too weak to explain the experimentally measured variation, a discrepancy that is worse if charging effects are taken into account.¹⁰ Moreover, the motion of JV's in this particular temperature-field regime is expected to be strongly damped due to the interaction with (unpinned) pancake vortices. We therefore seek an interpretation in terms of nearly immobile JV's. The increase of the JPR frequency must then be due to the enhancement of *c*-axis phase correlations by the in-plane field.³²

Phase correlations in the vortex liquid can be increased either by macroscopic segregation into PV-rich and PV-depleted zones, or alternatively, by local rearrangements of PVs to adjust to the presence of JVs, even in the vortex liquid state. As to phase segregation, recent magneto-optical imaging on overdoped $\text{Bi}_2\text{Sr}_2\text{CaCu}_2\text{O}_{8+\delta}$ for fields very closely aligned to the planes has shown that large inhomogeneities of the PV density can occur under the influence of an in-plane field.³³ We have performed the same experiment to verify that this is not the cause of the change of the JPR response. For low values of H^{\perp} , the field penetration is indeed inhomogeneous (Fig. 1). In particular, as in Ref. 34, the shape of the phase transformation front at first order vortex melting is affected by the direction of the in-plane field. The two field components are therefore not independent within the sample. However, once the vortex system is entirely transformed to the liquid phase, no contrast can be seen using the DMO technique. This means that inhomogeneity of B^{\perp} is less than our resolution (0.1 Oe) and cannot explain the changes of the JPR when an in-plane field is applied.

We therefore propose that PVs in the vortex liquid rearrange themselves on short length scales in order to coincide with JVs, yielding a novel correlated, PV density-modulated liquid. According to Bulaevskii¹⁹ and Koshelev,³ the Lorentz force exerted by the in-plane currents of JVs on a PV is balanced by the restoring force of the other pancakes. In the vortex solid, this balance results in a mutual attraction between a JV and a flux line, and the formation of the crossing-lattice structure.^{1,2} The range of this attractive interaction is of the order of $\lambda_J = \gamma s$. The energy gain per unit length due to a crossing event between a PV stack and a JV is $E_x = 4C_{solid}\varepsilon_0^2/\lambda_J^2 U_M$. Here, $U_M = C_{44}k_z^2/2n_v$ is the magnetic tilt stiffness of the pancake vortex stack,

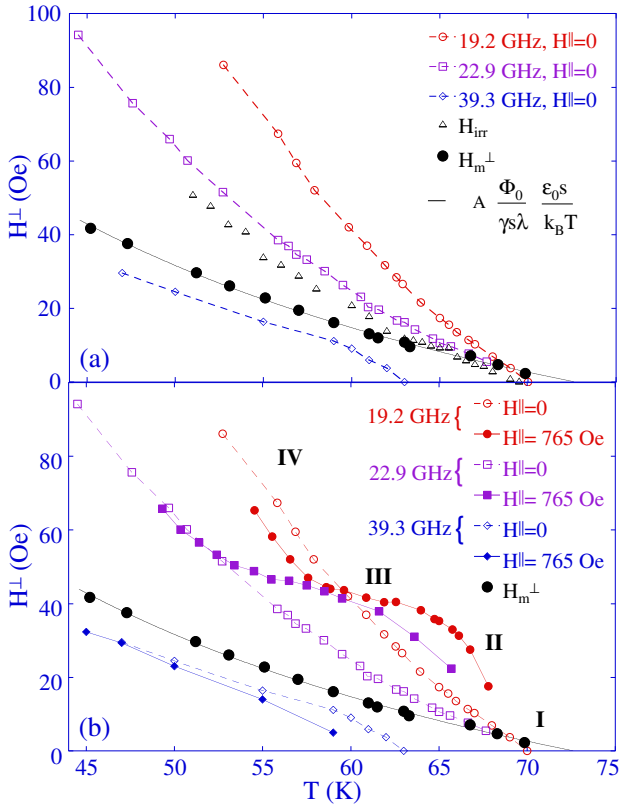


FIG. 7: (a) T -dependence of H_{JPR}^\perp obtained for 19.2, 22.9 and 39.3 GHz. The irreversibility line and the vortex lattice melting line for $H^\perp = 0$ are also reported. The fit of the melting line $H_m^\perp = A(\Phi_0/\lambda_J\lambda)(\epsilon_0 s/k_B T)$ is taken from Ref.²⁵ ($A \approx 1$) (b) Effect of H^\parallel on the JPR fields. For clarity, only results obtained for one value of the in-plane field for each frequency are shown. Labels I to IV refer to regimes described in the text and apply to the 19.2 and 22.9 GHz curves.

$C_{44} = B^\perp \epsilon_0 \ln [1 + r_{cut}^2 k_z^2 / (1 + r_w^2 k_z^2)] / 2\Phi_0 \lambda_{ab}^2 k_z^2$,³⁵ $n_v = a_0^{-2} = B^\perp / \Phi_0$, $k_z \approx \pi/s$ is the typical wavevector of the pancake stack deformation, $r_{cut} = \min(a_0, \lambda_{ab}) \approx \lambda_{ab}$, and C_{solid} a constant. The wandering length r_w describes the relative displacement of PVs in neighboring layers.³⁶ Carrying over the calculation to the vortex liquid, we find that E_x is particularly well estimated by these expressions. Namely, these disregard the Josephson coupling term in the vortex line tension, absent in the liquid.¹² However, r_w is not defined in the vortex liquid and should be replaced by $\sqrt{2\Phi_0(1 - \mathcal{C})/\pi B^\perp}$.³⁶ Also, we replace C_{solid} by C_{liquid} .

A comparison of the energy E_x/c_z gained from crossing events to the PV interaction energy $E_{int} = C_1 \epsilon_0 K_0(a_0/\lambda_{ab})$ shows that rearrangement of PVs in the vortex liquid so as to maximize the number of crossing events with JVs is favorable if

$$8\sqrt{\frac{\gamma B^\parallel}{\beta\Phi_0}} \left(\frac{\lambda_{ab}^2}{\gamma^2 s} \right) \sqrt{\ln \left(1 + \frac{\lambda_{ab}^2 \pi B^\perp}{2\Phi_0(1 - \mathcal{C})} \right)} > \tilde{C} K_0 \left(\frac{a_0}{\lambda_{ab}} \right) \quad (5)$$

Here, $K_0(x)$ is the modified Bessel function, c_z is the JV lattice (JVL) spacing along the c -axis,³⁷ and $\tilde{C} = C_1/C_{liquid}$. Even though the inequality (5) is implicit

because of the dependence of \mathcal{C} on the crossing energies, it can be evaluated using the experimental values of \mathcal{C} at a given measuring frequency.

Solving Eq. (5) for $B^\perp(T)$, we obtain correlated-homogeneous vortex liquid boundaries for different values of the in-plane field, see Fig. 5. Here, we have taken $\lambda_{ab}(T) = \lambda_{ab}(0)/\sqrt{1 - (T/T_c)^4}$, with $\lambda_{ab}(0) = 300$ nm.¹² For $\tilde{C} = 2.6$, these boundaries coincide with the loci of f_{pl} in regimes II and III, which in turn correspond to the lines on which \mathcal{C} for non-zero H^\parallel has dropped back to the value observed near the melting line in the absence of an in-plane field. Thus, the observed increase of $H_{JPR}^\perp(T)$, and consequently, of the interlayer phase correlations, is fully consistent with the existence of a correlated vortex liquid in the region delimited by the dashed and drawn lines of Fig. 5, the extent of which grows with increasing H^\parallel . In the correlated liquid, the attraction between PVs and JVs leads to a spatially modulated PV density: in the vicinity of JV stacks, the mean distance between PVs is smaller than in JV-free regions. The c -axis phase coherence of this state is higher than that of the vortex liquid for $H^\parallel = 0$ because of the depletion of PVs in the regions between JV stacks. The demise of the correlated liquid at high T (regime II) is caused by the decrease with temperature of the inter-pancake vortex repulsion, less rapid than that of the PV-JV attraction. The disappearance of the correlated liquid when H^\perp is increased is very sudden, as testified by the close proximity of the resonant fields for $f = 19.2$ and 22.9 GHz in regime III [Fig. 7(b)]. This shows that the phase coherence in the plateau-regime is nearly constant, and then rapidly drops as the PV density is increased.

The modification of the lineshape of the JPR absorption supports our interpretation. Fig. 3(c) shows that the maximum absorption at $f = f_{pl}$ in regime II decreases linearly as function of H^\parallel . This is explained by the presence of well-defined JVs. Namely, the plasma oscillation is impeded in the vicinity of the non-linear JV cores because of the rapid 2π -modulation, with period c_z , of the gauge-invariant phase ϕ along the c -axis. The resulting decrease in dissipation is given by the ratio $\lambda_{J\parallel} H^\parallel / \Phi_0$ of the volume occupied by the JVL (*i.e.* that does not participate in the JPR), to the volume of the sample. Cooper pairs located in JV-free regions still exhibit plasma oscillations as long as the separation c_y between JVs is larger than $L_\phi = \lambda_J^2 / a_0$.³² This is well satisfied: for our in-plane field range, $260 < H^\parallel < 1100$ Oe, $c_y \approx (5 - 10)L_\phi$. It should be noted that the coefficient of the linear decrease of absorption is ten times higher than expected. This is, possibly, because the width of JV-core region affecting the JPR is larger than λ_J .

The measurements also show that the low-field flank of the absorption peak decreases with H^\parallel , whereas the high field tail is only pushed slightly upwards. In the vortex liquid state, the low field part of the JPR absorption comes from localized JPR modes over wide areas of the sample.³² However, the presence of a JVL prevents the occurrence of homogeneous Josephson coupling over such areas. The high field part of the absorption arises from contributions of small fluctuating areas over which

Josephson coupling is established in a hap-hazard way. These local contributions are not destroyed by the JVL.

Finally, we address the low temperature region IV, in which the main JPR absorption peak lies above the postulated correlated-homogeneous vortex liquid boundary. From the height of the absorption peak, which is nearly H^{\parallel} -independent and close to what is observed in $H^{\parallel} = 0$, we conclude that the whole sample volume contributes to the plasma resonance. This is consistent with the absence of Josephson vortices, the formation of which is inhibited by pancake vortex fluctuations. The JPR is best described by the high temperature expansion of Refs. 18,32.

On the other hand, the low H^{\perp} peak, which corresponds to the “low-temperature mode” of Refs. 17,26, occurs only in the vortex solid and in the correlated vortex liquid. It is therefore related to the existence of well-defined JV’s. We note that the very weak H^{\parallel} -dependence of this peak seems to contradict the H^{\perp} -independent, $\sim H^{\parallel -2}$ dispersion of the predicted antiphase mode with $q_{\perp} = \pi/s$.¹³

V. SUMMARY AND CONCLUSION

In summary, the effect of an in-plane magnetic field on microwave dissipation near the longitudinal Josephson Plasma Resonance in underdoped $\text{Bi}_2\text{Sr}_2\text{CaCu}_2\text{O}_{8+\delta}$ is closely correlated to the thermodynamical state of the underlying vortex system, and, in particular, to the effectiveness of pancake vortex pinning. In the vortex solid,

the application of an in-plane field slightly suppresses the perpendicular field at which the JPR takes place. In contrast, the application of an in-plane field in the presence of perpendicular fields exceeding the first order melting transition can lead to a correlated, PV density-modulated vortex liquid. The overall phase coherence of this phase is higher than the coherence of the usual vortex liquid state because a substantial fraction of pancakes is aligned on stacks of Josephson vortices. The existence of well-defined Josephson vortices, and therefore, of a correlated liquid, requires the integrity of PV stacks over, at least, the distance c_z separating Josephson vortices in the same stack along the c -axis; hence, it is only possible for low densities of PVs, close to the melting line. Our results therefore constitute evidence for the “linelike nature” of the vortex liquid close to the melting line in $\text{Bi}_2\text{Sr}_2\text{CaCu}_2\text{O}_8$, similar to the “linelike liquid” reported in Ref. 38 for less anisotropic layered $\text{Tl}_2\text{Ba}_2\text{CaCu}_2\text{O}_8$. The correlated-homogeneous vortex liquid boundary is also reminiscent of recent results showing a transition from a linelike liquid to a phase without vortex line tension in $\text{YBa}_2\text{Cu}_3\text{O}_{7-\delta}$.³⁹

VI. ACKNOWLEDGEMENTS

We thank J. Blatter, A.E. Koshelev, D. van der Marel, and T. Shibauchi for useful discussions. One of us (P.G.) was partially supported by MNiSW-grant no. N202 058 32/1202.

¹ A. Grigorenko, S. Bending, T. Tamegai, S. Ooi, and M. Henini, *Nature (London)* **414**, 728 (2001).

² T. Matsuda, O. Kamimura, H. Kasai, K. Harada, T. Yoshida, T. Akashi, A. Tonomura, Y. Nakayama, J. Shimoymaya, and K. Kishio, *Science* **294**, 2136 (2001).

³ A. E. Koshelev, *Phys. Rev. Lett.* **83**, 187 (1999).

⁴ C. A. Bolle, P. L. Gammel, D. G. Grier, C. A. Murray, D. J. Bishop, D. B. Mitzi, and A. Kapitulnik, *Phys. Rev. Lett.* **66**, 112 (1991).

⁵ E. Zeldov, D. Majer, M. Konczykowski, V. B. Geshkenbein, V. M. Vinokur, and H. Shtrikman, *Nature (London)* **375**, 373 (1995).

⁶ B. Schmidt, M. Konczykowski, N. Morozov, and E. Zeldov, *Phys. Rev. B* **55**, R8705 (1997).

⁷ S. Ooi, T. Shibauchi, N. Okuda, and T. Tamegai, *Phys. Rev. Lett.* **82**, 4308 (1999).

⁸ M. Konczykowski, C.J. van der Beek, A.E. Koshelev, V. Mosser, M. Dodgson, and P.H. Kes, *Phys. Rev. Lett.* **97**, 237005 (2006).

⁹ Y. Matsuda, M. B. Gaifullin, K. Kumagai, K. Kadowaki, and T. Mochiku, *Phys. Rev. Lett.* **75**, 4512 (1995).

¹⁰ M. Tachiki, T. Koyama, and S. Takahashi, *Phys. Rev. B* **50** 7065 (1994).

¹¹ A. E. Koshelev, L.N. Bulaevskii, and M.P. Maley, *Phys. Rev. Lett.* **81**, 902 (1998).

¹² S. Colson, M. Konczykowski, M. B. Gaifullin, Y. Matsuda, P. Gierlowski, M. Li, P. H. Kes, and C. J. van der Beek, *Phys. Rev. Lett.* **90**, 137002 (2003).

¹³ A. E. Koshelev, arXiv:0705.2239v1 [cond-mat.supr-con], (2007).

¹⁴ O.K.C. Tsui, in *Spectroscopic Studies of Superconductors*, ed. I. Bozovic and D. van der Marel, S.P.I.E. Bellingham (1996).

¹⁵ Y. Matsuda, M. B. Gaifullin, K. Kumagai, K. Kadowaki, T. Mochiku, and K. Hirata, *Phys. Rev. B* **55**, R8685 (1997).

¹⁶ S.P. Bayrakci, O.K.C. Tsui, N.P. Ong, K. Kishio, and S. Watauchi, *Europhys. Lett.* **46**, 68 (1999).

¹⁷ I. Kakeya, T. Wada, R. Nakamura, and K. Kadowaki, *J. Low Temp. Phys.* **117**, 611 (1999).

¹⁸ A. E. Koshelev, *Phys. Rev. Lett.* **77**, 3901 (1996).

¹⁹ L. N. Bulaevskii, M. Maley, H. Safar, and D. Domínguez, *Phys. Rev. B* **53**, 6634 (1996).

²⁰ N. Morozov, M. Maley, L. N. Bulaevskii, V. Thorsmølle, A. E. Koshelev, A. Petrean, and W. K. Kwok, *Phys. Rev. Lett.* **82**, 1008 (1999).

²¹ M. Li, C. J. van der Beek, M. Konczykowski, A. A. Menovsky, and P. H. Kes, *Phys. Rev. B* **66**, 024502 (2002).

²² A. Soibel, E. Zeldov, M. Rappaport, Y. Myasoedov, T. Tamegai, S. Ooi, M. Konczykowski, and V. B. Geshkenbein, *Nature (London)* **406**, 282 (2000).

²³ C. J. van der Beek, I. Abal’osheva, M. Konczykowski, M. Li, P. H. Kes and M. V. Indenbom, in *Magneto-Optical Imaging*, edited by T.H. Johansen and D. Shantsev (Kluwer Academic Publishers, pp 79–86, 2004).

²⁴ N. Morozov, E. Zeldov, D. Majer, and M. Konczykowski,

Phys. Rev. B **54**, R3784 (1996).
²⁵ G. Blatter, V. Geshkenbein, A. Larkin, and H. Nordborg, Phys. Rev. B **54**, 72 (1996).
²⁶ I. Kakeya, T. Wada, R. Nakamura, and K. Kadowaki, Phys. Rev. B **72**, 014540 (2005).
²⁷ T. W. Li, A. A. Menovsky, J. J. Franse, and P. H. Kes, Physica C **257**, 179-186 (1996).
²⁸ The observed increase of H_{JPR}^\perp with H^\parallel is much weaker or absent in more disordered crystals in which the irreversibility line lies above the measured Josephson Plasma Resonance peaks.
²⁹ H. Enriquez, N. Bontemps, P. Fournier, A. Kapitulnik, A. Maignan, and A. Ruyter, Phys. Rev. B **53**, R14757 (1996).
³⁰ Y. I. Latyshev, A. E. Koshelev, and L. N. Bulaevskii, Phys. Rev. B **68**, 134504 (2003).
³¹ A. E. Koshelev, Y. I. Latyshev, and M. Konczykowski, Phys. Rev. B **74**, 104509 (2006).
³² A. E. Koshelev, L. N. Bulaevskii, and M. P. Maley, Phys. Rev. B **62**, 14403 (2000).
³³ S. Kasahara, Y. Tokunaga, N. Kameda, M. Tokunaga, and T. Tamegai, Phys. Rev. B **71**, 224505 (2005).
³⁴ M. Yasugaki, K. Itaka, M. Tokunaga, N. Kameda, and T. Tamegai, Phys. Rev. B **65**, 212502 (2002).
³⁵ A. E. Koshelev and P. H. Kes, Phys. Rev. B **48**, 6539 (1993).
³⁶ A. E. Koshelev and L. N. Bulaevskii, Physica C **341-348**, 1503 (2000).
³⁷ L. J. Campbell, M. M. Doria, and V. G. Kogan, Phys. Rev. B **38**, 2439 (1988).
³⁸ V.K. Thorsmølle, R.D. Averitt, M.P. Maley, M.F. Hundley, A.E. Koshelev, L.N. Bulaevskii, and A. J. Taylor Phys. Rev. B **66**, 012519 (2002).
³⁹ F. Bouquet, C. Marcenat, E. Steep, R. Calemczuk, W. Kwok, U. Welp, G. Crabtree, R. Fisher, N. Phillips, and A. Schilling, Nature **411**, 448 (2001).

